Astronomy & Astrophysics manuscript no. isw˙stack˙voids
January 25, 2013

On the detection of the integrated Sachs-Wolfe effect with stacked voids

Stéphane Ilić, Mathieu Langer, Marian Douspis

(Affiliations can be found after the references)

Preprint online version: January 25, 2013

ABSTRACT

The stacking of Cosmic Microwave Background (CMB) patches has been recently used to detect the integrated Sachs-Wolfe effect (iSW). Focusing on the locations of superstructures they identified in the Sloan Digital Sky Survey (SDSS), Granett et al. (2008a) found a signal with strong significance and an amplitude reportedly higher than expected within the ΛCDM paradigm. We revisit the analysis using our own robust protocol, and extend the study to the two most recent and largest catalogues of voids publicly available (Pan et al. 2012, Sutter et al. 2012). We quantify and subtract the level of foreground contamination in the stacked images and we determine the contribution on the largest angular scales from the first multipoles of the CMB. We obtain the radial temperature and photometry profiles from the stacked images. Using a Monte Carlo approach, we compute for each catalogue the statistical significance of the profiles and identify the angular scale at which the signal-to-noise ratio (SNR) is maximal. While we essentially confirm the signal detection reported by Granett et al., we do not find anything significant with the other two catalogues. A rescaling of the voids to the same size on the stacked image does not improve the results. We stress the importance of a posteriori selection effects that might arise when intending to increase the SNR, and we discuss the possible impact of void overlap and alignment effects. We argue that the interpretation in terms of an iSW effect of any detected signal via the stacking method is far from obvious.

Key words. cosmology: cosmic background radiation – cosmology: dark energy – cosmology: large-scale structure of the Universe

1. Introduction

Among the many sources of secondary anisotropies of the Cosmic Microwave Background (CMB) temperature (for a recent review, Aghanim et al. 2008), the integrated Sachs-Wolfe (henceforth iSW, Sachs & Wolfe 1967) effect is particularly interesting in connexion with the acceleration of cosmic expansion. In principle, in a universe not dominated by cold matter, the energy of CMB photons is redshifted or blueshifted while they travel across cosmic over-densities or under-densities respectively due to the stretching-out of the gravitational potentials created by the structures. Since the amplitude of this effect is expected to be rather small and showing mostly on the largest angular scales (due to a line-of-sight cancellation, Kofman & Starobinskii 1985), it has been suggested, first in the context of studies of the Rees-Sciama effect (Crittenden & Turok 1996), to cross-correlate the CMB temperature fluctuations with the distribution of tracers (e.g. galaxies) of gravitational potentials. After the first attempts to detect the iSW effect by that method (Boughn et al. 1998; Boughn & Crittenden 2002), many studies have been published using the latest galaxy survey data. Remarkably, often based on similar data and comparable techniques, the claims for detection range from a "negligible" to a $\sim 4.5\sigma$ statistical significance (for a discussion, see Dupé et al. 2011, and Giannantonio et al. 2012).

This puzzling situation calls for a clarification. Discussions of the cross-correlation methods and techniques set aside, it would be invaluable to have an other way to evidence the iSW effect. One such way would be to measure it directly in the CMB maps at the locations of the gravitational potentials that are responsible for it. Unfortunately, its amplitude with respect to the primary CMB anisotropies does not allow us to detect it structure by structure. However, stacking techniques can be profitably adopted to enhance the signal-to-noise ratio. Using the Wilkinson Microwave Anisotropy Probe (WMAP) 5 year maps (Hinshaw et al. 2009), such a technique has been applied by Granett et al. (2008a) to supervoids and superclusters they identified in the catalogue of Luminous Red Galaxies (LRGs) in the Data Release 6 (DR6) of the Sloan Digital Sky Survey (SDSS) (see also Granett et al. 2008b). Their super-structure identification method uses the VOBOZ (VOronoi BOund Zones, Neyrinck et al. 2005) and ZOBOV (ZOnes Bordering On Voidness, Neyrinck 2008) Voronoi tessellation based, publicly available numerical codes. Focusing on the most significant (in terms of the density contrast) 50 supervoids and 50 superclusters, Granett et al. (2008a, see also Hernández-Monteagudo & Smith 2012) reported a combined mean temperature deviation of 9.6 μK, at a significance just above 4σ, which they interpret as a signature of the iSW effect.

Using the Millennium simulation (Springel et al. 2005) and measuring the iSW effect that is expected in a standard ΛCDM universe, Granett et al. (2008a) found that it is $\sim 2\sigma$ lower, at 4.2 μK, than what they obtained from the WMAP data. Other studies have also measured an iSW effect somewhat higher than expected (e.g. Giannantonio et al. 2008; Ho et al. 2008; Giannantonio et al. 2012), although with a small statistical significance. The high significance and the stronger than expected amplitude of the iSW effect detected through stacking have stimulated a number of investigations. For instance, Hunt & Sarkar (2010) argue that LRGs need to be unnaturally *underbiased* tracers of matter if we want to attribute the signal measured by Granett et al. (2008a) to the iSW effect in the standard ΛCDM model. Nadathur et al. (2012) carefully analysed possible biasing effects arising from the strategy adopted by Granett et al. (2008a), but showed that even when those selection effects are taken into account, the signal from supervoids expected within standard ΛCDM is still at odds by $> 3\sigma$ with

the value measured by Granett et al. (2008a, for similar conclusions reached with numerical simulations of the iSW effect, see Flender et al. 2012) . On the other hand, Pápai & Szapudi (2010) described the superstructures by uncompensated density profiles from Gaussian statistics and found that large temperature deviations, $\Delta T \sim 10\mu$K, can be obtained. Moreover, building on this result, Pápai et al. (2011) re-assessed the statistical significance of those values and estimated that the discrepancy between the observations and the theoretical ΛCDM predictions is 2σ. However, as noted in Nadathur et al. (2012), the latter interpretation would imply voids with unphysical, $\delta < -1$, underdensities. Finally, let us note that Granett et al. (2009) re-analysed with a template fitting method the WMAP 5 CMB data and confirmed the 4σ significance of the signal found previously. Furthermore, they also reconstructed an iSW map from the very same LRG sample they used for their previous superstructure identification. On that reconstructed map, however, the combined voids and clusters associated temperature deviation was only $0.08 \pm 0.1\mu$K, casting a doubt on the suggestion that the signal is indeed due to the linear iSW effect.

Should we conclude that the large CMB temperature deviations measured in association with superstructures signal a tension with the ΛCDM model? In this paper, we would like to take a new step towards answering that question. Since the study of Granett et al. (2008a), new CMB maps have been released and other superstructure catalogues have been published. We do the stacking analysis with the new data and look for the iSW signal that could be associated with the large scale structure. We pay a particular attention to the bias introduced into the results by selection effects and illustrate it with an explicit example. We begin by introducing the data used for this study. In Section 3, we outline the methodology we adopted, stressing the assessment of the statistical significance of our results. The latter are detailed in Section 4, and in Section 5 we discuss the importance of a posteriori selection effects that may artificially boost the statistical significance. Finally, we conclude in Section 6. We use the parameters from WMAP 7 best-fit cosmology for all relevant calculations.

2. The data

2.1. Cosmic Microwave Background

In the present study, we use the maps of the Cosmic Microwave Background released by the WMAP team after seven years of observation (Jarosik et al. 2011), in contrast to the five-year data used by Granett et al. (2008a, Gr08 thereafter) in their study. We take the individual channel maps at the three frequencies that are the less contaminated by foregrounds (the Q, V and W bands at 41, 61 and 94 GHz respectively). We also use the hit map of the WMAP mission, i.e. the map which contains for each pixel the number of times it was observed in the satellite lifetime. The impact of foregrounds and the associated possibility of false signals is often a source of uncertainty in iSW studies ; we will therefore consider and assess their possible influence by redoing our analyses on the foreground reduced maps released by the WMAP team in the same frequency channels.[1]

2.2. Granett et al. (2008)

The first catalogue of superstructures (clusters and voids) that we consider is that created and studied by Gr08 : As it was already explored with WMAP 5-year data, it will serve us as a "fiducial" set when testing all the steps of our own stacking procedure. This will also be the opportunity to revisit the work of Gr08 with the newer 7-year data from WMAP.

The catalogue is based on the LRG sample of the SDSS DR6 (Adelman-McCarthy et al. 2008), which is composed of 1.1 million LRGs in the range $0.4 < z < 0.75$ (with a median $z = 0.52$) and covers 7500 square degrees on the sky and occupies a volume of $\sim 5\ h^{-3}Gpc^3$. In this survey, Gr08 searched for clusters and voids using respectively the two publicly-available structure-finding algorithms VOBOZ and ZOBOV based on Voronoi tessellation. They detected 631 voids and 2836 clusters above a 2σ "significance level", defined as the probability of obtaining in a uniform Poisson point sample the same density contrasts as those of voids and clusters.

From these results, they kept and released only the 50 most significant clusters and 50 voids, which they used in their CMB stacking analysis. The catalogue of these 100 superstructures contains all the information needed for their analysis. For each structure it provides : the position of its centre on the celestial sphere, the mean and maximum angular distances on the sky between the galaxies in the structure and its centre, its physical volume, and three different measures of its density contrast (either calculated from all its Voronoi cells, from only its over/underdense cells, or from only its most over/underdense one).

After conversion to physical distances (see details in Section 2.5), we note that these voids have a mean effective radius of about 78 Mpc and a mean redshift of ~ 0.5, corresponding to angular sizes on the sky of about 3.5 degrees.

2.3. Pan et al. (2012) void catalogue

Pan et al. (2012) published a catalogue of cosmic voids and void galaxies identified in the seventh data release (DR7) of the SDSS. Using the VoidFinder algorithm as described by Hoyle & Vogeley (2002), they identified and catalogued 1055 voids with redshifts lower than $z = 0.1$. They provide for each void its position on the sky (also, but not useful for us, its 3D position in the survey), its physical radius (defined as the radius of the maximal sphere enclosing the void), an effective radius (as voids are often found to be elliptical) defined as the radius of a sphere of the same volume, its physical distance to us, its volume and mean density contrast.

The filling factor of the voids in the sample volume is 62%. The largest void is just over 47 Mpc in effective radius while their median effective radius is of about 25 Mpc. Some of them are both very close to us and relatively large (more than 30 Mpc in radius) resulting in large angular sizes on the sky, up to 15 degrees and above.

2.4. Sutter et al. (2012) void catalogue

The most recent catalogue considered in the present study was released by Sutter et al. (2012).[2] Using their own improved version of the void finding algorithm ZOBOV, Sutter et al. also built a void catalogue from the SDSS DR7, taking particular care of

[1] All maps can be downloaded from the LAMBDA website http://lambda.gsfc.nasa.gov

[2] Catalogue published on-line at http://www.cosmicvoids.net, version 16/08/2012.

Table 1. Summary of the Sutter et al. catalogue and its subsamples, as well as of the catalogues of Granett et al. and Pan et al..

(Sub)sample name	Redshift range	Number of voids
dim1	$0.005 < z < 0.046$	97
dim2	$0.05 < z < 0.1$	360
bright1	$0.1 < z < 0.15$	287
bright2	$0.15 < z < 0.19$	146
lrgdim	$0.17 < z < 0.34$	224
lrgbright	$0.39 < z < 0.41$	32
Total	$0.005 < z < 0.41$	**1146**
Granett et al.	$0.43 < z < 0.69$	**50**
Pan et al.	$0.009 < z < 0.1$	**1055**

accounting for the effects of the survey boundary and masks. They found a total of 1146 voids which they divided into six distinct subsamples of increasing redshift : four from the main SDSS (named *dim1*, *dim2*, *bright1* and *bright2*) and two from the SDSS LRG sample (*lrgdim* and *lrgbright*). The redshifts of these voids span $z \sim [0, 0.4]$ while their sizes range approximatively from 10 to 180 Mpc ; a summary of the six subsamples and their contents is provided in Table 1, together with the contents of the other two catalogues described in Sections 2.2 and 2.3.

This catalogue stands out by the amount of information provided about its voids : position of the barycentre, redshift, effective radius (with the same definition as in the Pan et al. catalogue), locations of member galaxies, one-dimensional radial profiles of stacked voids, two-dimensional projections of stacked voids and other statistical information about their distribution.

2.5. Using the void catalogues

The only indispensable information that we extract from these catalogues are the positions on the sky of the observed structures (most frequently the position of their barycentre), an essential information needed to apply the stacking procedure : they are most often provided in celestial coordinates (RA, DEC) that we easily convert into galactic coordinates in order to use them in the framework of the HEALPix suite. For more advanced analysis and interpretations, we first require the redshift of these structures : this parameter is directly given in the considered catalogues, except for that of Pan et al. where we obtained it from the physical distance to the voids. Finally we also make use of the physical radius of the structures, through its relation to the angular size on the sky (see Section 5.2). When provided, we use the effective radius of the structure (Pan et al., Sutter et al.) which we translate into an angular size using the available redshift information. For the Gr08 catalogue, we derive the effective radius – with the same definition as in the two other catalogues – from the provided volume, and then also convert it to an angular size. This is somewhat a compromise between the two angular sizes already provided by Gr08 : the *mean radius* between the centre of the void and all its Voronoi cells (likely an underestimate of the void size on the sky), and the maximum radius between the centre and the farthest cell (likely an overestimate).

Of the Gr08 catalogue, we will only use the voids and disregard the clusters, both for the sake of consistency with the other two catalogues, but also because voids are more adapted for stacking studies : indeed, emission of astrophysical origin is less likely to contaminate the iSW signal from these objects. As a summary, we plot the features of the voids from all catalogues in Fig. 1, including their redshifts, effective radii and corresponding angular sizes.

3. Methodology

3.1. Initial procedure

The analysis of these three different catalogues requires us to have a robust and well defined procedure for a systematic analysis of all the structures considered. First, the standard stacking procedure that we apply in this study consists in the following steps, for each superstructure sample or subsample :

- We first take a CMB map of the WMAP data at a given frequency, either raw of foreground cleaned, from which we remove the cosmological monopole and dipole;
- We construct the associated weight map by taking a galactic mask (here the KQ75 from the WMAP team, the extended mask for temperature analysis removing $\sim$ 22% of the sky along the galactic plane and around point sources) and multiplying it by the hit map associated with the survey ;
- We retrieve the galactic longitudes and latitudes of the structures we study ;
- We use a custom code based on the HEALPix[3] package in order to cut a patch in the CMB map centred around each structure. We choose the patches to have a 6 arcmin/pixel resolution (small enough to oversample any of the CMB maps used) and to be squares of 301×301 pixels, i.e. $30° \times 30°$ patches ;
- At the same time, we cut identical square patches at the same locations in the associated weight map ;
- The final stacked image is then constructed as the average image of all CMB patches weighted by their corresponding weight patches.

Two main products are then extracted from the stacked image :

- the radial temperature profile starting from the centre of the image, by computing the mean temperature of the pixels in rings of fixed width and increasing angular radius. Considering the characteristics of our stacked images, it is calculated here for 150 radii between 0° and 15°, with a width of $\Delta\theta = 0.1°$;
- the aperture photometry profile, using a compensated filter approach : At each chosen angle θ, we compute the photometry as the difference between the mean temperature of the pixels inside the disk of angular radius θ and the temperature of the pixels in the surrounding ring of same area, i.e. the ring enclosed between circles of radii θ and $\theta\sqrt{2}$. With this procedure, we obtain this profile for 150 angles between 0° and $(15/\sqrt{2}) \sim 10.6°$.

The summation of square pixels contained inside a disk can lead to calculation errors due to omitted fractions of pixels close to the boundaries of the disk. To reduce these as much as possible, we upscale the 301×301 stacked image into a 1204×1204 one – each pixel of the original image is divided into 16 sub-pixels of the same value. Statistical errors for these two profiles are estimated by computing the standard deviation of each calculated mean of pixels. We mainly focus on the analysis of these two profiles (the image itself is useful for illustration purposes only), where we look for any remarkable signal whose significance we assess below (see Section 3.3).

[3] http://healpix.jpl.nasa.gov

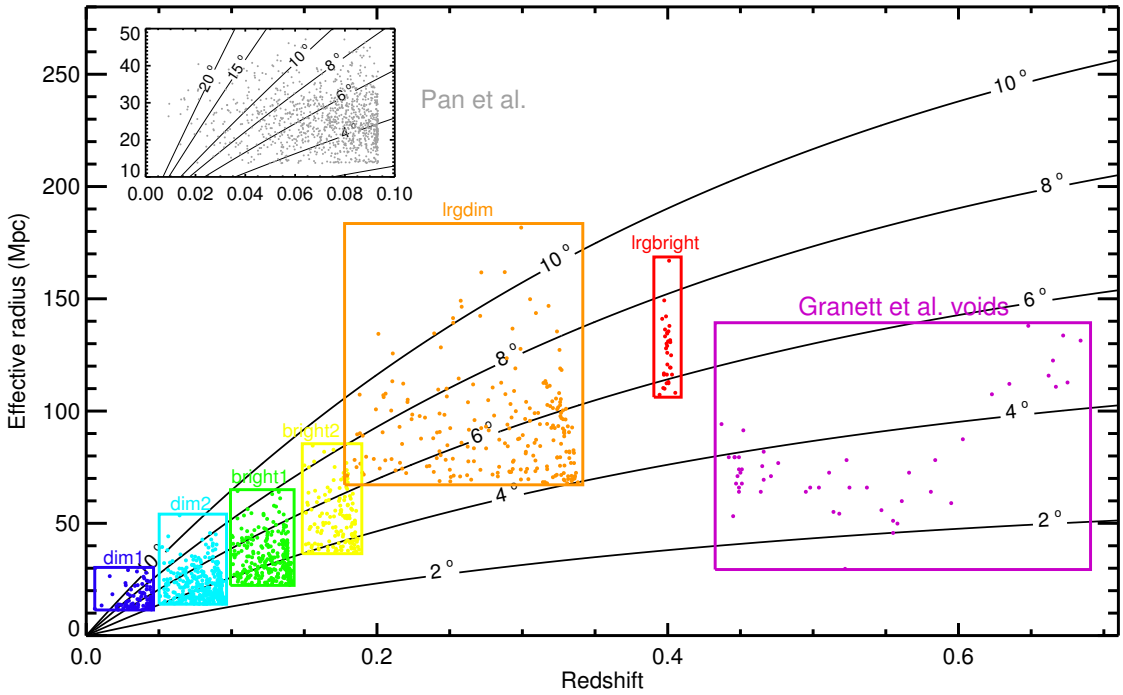

Fig. 1. Effective radii (in Mpc) as a function of redshift for all the voids used in this work. The two catalogues of Granett et al. and Pan et al, and the six subsamples of Sutter et al. are delimited by boxes labelled by their names. The black curves are here to indicate the angular size (in degrees) of a structure in the redshift-radius plane.

We note that the chosen size of the CMB patches is large enough to enclose any of the structures studied and to properly compute their photometry (based on the effective angular radius which has to be smaller than $(15/\sqrt{2})°$), with the exception of 15 voids (out of 1146) in the Sutter et al. catalogue and 21 in the Pan et al. one (out of 1055); we will omit these voids in the stacking.

3.2. Choice of maps

Each of the three CMB maps that we use (WMAP Q, V and W) inherently has a different resolution and contains different types and levels of foregrounds which may contaminate them. Before progressing any further, we assess the impact of the properties of each map, using our fiducial stacking (i.e. using the Gr08 void positions) as a basis.

3.2.1. Effects of resolution

We perform the fiducial stacking of the Gr08 voids on the three raw CMB maps from the Q, V and W frequency bands, the beam sizes of which are respectively 30.6, 21 and 13.2 arcminutes ; an example of a stacked image is shown in Fig. 2. In order to have a consistent stacking analysis through all the considered frequencies, we need to "standardise" those maps : we first smooth the maps at the lowest resolution of the three (the Q band map) in order to lose as less information as possible. We then redo the fiducial analysis, and the resulting profiles are plotted in Fig. 3.

The stacks at each frequency, both raw and smoothed, give roughly the same results with only percent-level differences especially for the photometry profiles – the most useful products here. The degradation of the V and W maps to the lower resolution of the Q map naturally smooths the measured profiles and reduces their dispersion around the results of the Q band, which is the desired effect as we tried to standardise our results. Otherwise, this procedure does not modify significantly their amplitude and angular dependence, so that we may adopt hereafter this new common resolution for all frequencies.

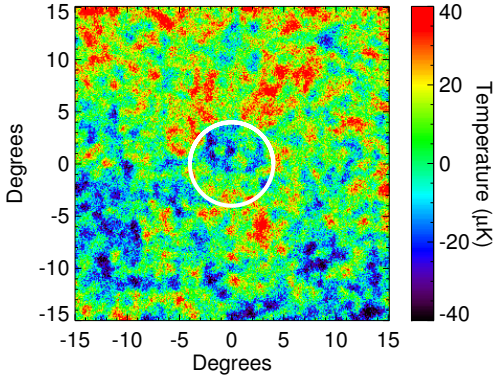

Fig. 2. Image resulting from our stacking procedure at the location of the 50 voids of Gr08, here using the V band CMB map of WMAP. A cold spot, reportedly due to the iSW effect, is visible roughly at the centre of the image with an angular radius of about 4° (underlined by the 4° radius white circle centred on the image).

In all cases, a signal appears in the photometry profile with a maximum at an angular scale of about 3.5°, the preferred size changing only very slightly between frequencies. We keep in mind that the smoothing procedure with a ∼ 30.6 arcminute beam erases the information and details contained below this scale. Therefore we should not devote much attention to any feature in the profiles at angles lower than this value.

3.2.2. Assessment of the effects of the foregrounds

One other source of concern comes from the influence of foregrounds present in the CMB maps, as they may mimic the expected iSW signal in the stacked images. To assess their possible

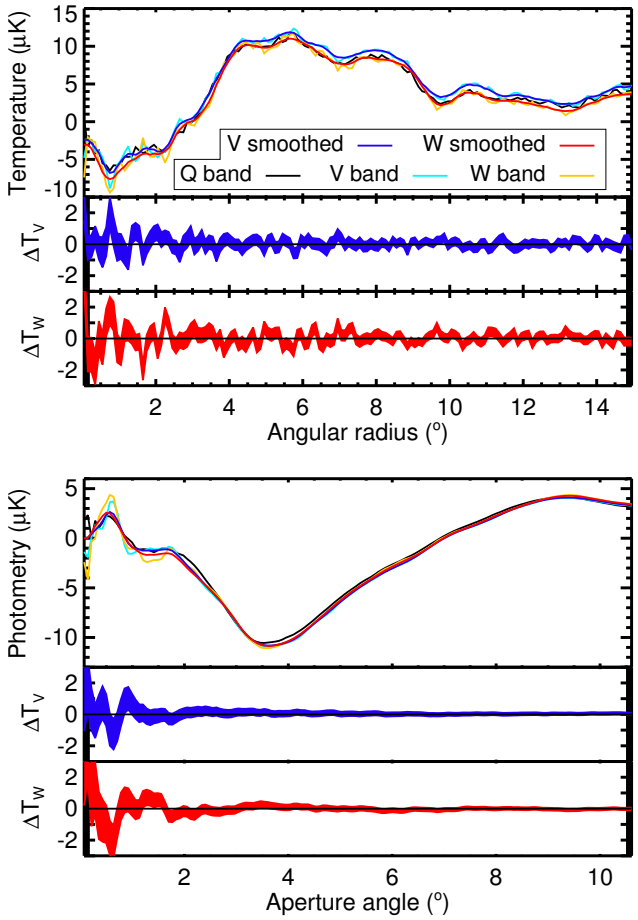

Fig. 3. *First plot* : radial temperature profiles (*top panel*) of the stacking of Gr08 voids, done on WMAP Q, V and W maps (both in native resolution and smoothed by a 30.6 arcminutes kernel). The differences in the profiles between the smoothed and original maps are plotted below the main plot (*middle :* V band, *bottom* : W band). The width of the shaded curves corresponds to the statistical errors on the profile measurements. *Second plot* : Same graphs and legend as above but for the aperture photometry profiles of the stacking of Gr08 voids.

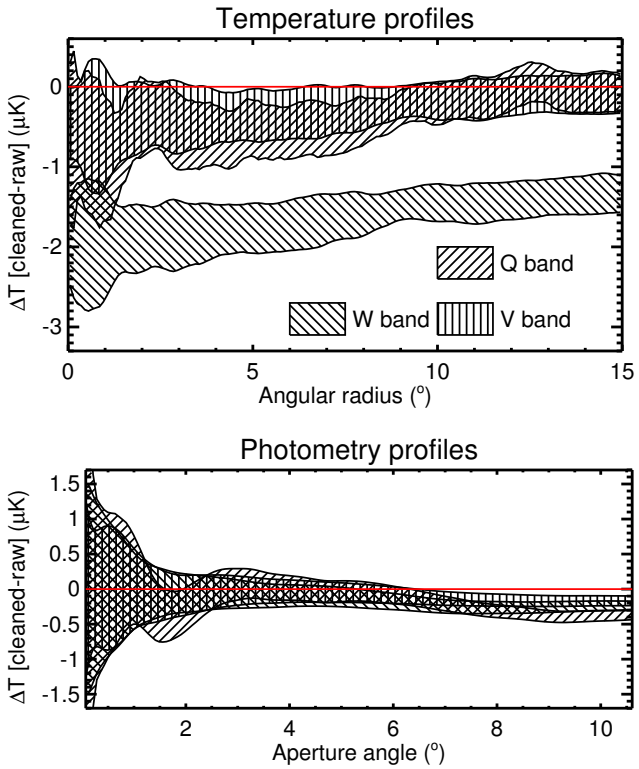

Fig. 4. For the Gr08 stacking, differences in the temperature (*top*) and photometry (*bottom*) profiles between foreground cleaned maps and raw maps, for the three frequency bands considered. The width of the shaded curves corresponds to statistical errors on the profile measurements. The quasi-flat offsets observed in the temperature profiles do not affect substantially the photometry.

impact, we perform the stacking of the Gr08 voids first on raw and then foreground cleaned CMB maps at all frequencies. We then look for differences between the two results, either in the amplitude or in the shape of the signal.

Results are illustrated in Fig. 4 : we obtain systematic offsets of a few micro-kelvins in the radial temperature profiles and less in the photometry profiles. This indicates that we mainly remove an almost uniform background, which does not influence much the aperture photometry of the stacked image. As a precaution we then use the foreground cleaned maps for our analyses. Possible residuals in the cleaned maps should not be of any concern since they would have the same "flat" behaviour in the stacked images.

3.2.3. Analysis of the temperature gradient

Another map-related problem showed up during our investigations, when we observed that a clear temperature gradient appeared in many of our stacked images with the new catalogues, roughly on a North-South axis with hotter high latitudes (see an example in Fig. 5). Foregrounds as a possible source of this can be excluded, because the gradient appears in both raw and foreground cleaned maps, and also to a lesser extent because it is contrary to our intuition about foreground contamination since we expect hotter temperatures closer to the galactic plane. One may wonder why this gradient was not observed by Gr08, but this can be explained by the fact that they rotated the CMB patches before stacking them in order to align the major axes of the voids. Introducing such rotations (which are a priori random statistically speaking) is enough to erase any systematic gradient. In our study, we did not have access to the information on the orientation of the voids (it is not included in the Gr08 catalogue) and we therefore did not rotate the CMB patches. A systematic gradient in the final image is clearly observed (see Figs. 2 and 5).

After discarding foregrounds as culprits, we looked for "intrinsic" causes of this gradient. This led us to decompose the CMB maps on the spherical harmonics and to analyse the individual contribution of each multipole. This approach proved fruitful as it appears that the measured gradient is mainly caused by the first few multipoles of the CMB maps we use, especially by the $\ell = 6$ multipole map. In the region of the sky covered by the SDSS (where all the superstructures we considered are located), these multipoles combine to yield indeed a strong North-South gradient (see Fig. 6) which will be present at some level in every patch of CMB, and therefore in the final stacked image.

Visually speaking, subtracting the contribution of these multipoles out of the CMB maps does effectively remove the gradient in the stacked image. But on the other hand, the effect is almost negligible in the photometry profile : indeed, the removed contribution has most often the shape of a simple tilted plane (see Fig. 5 for an example) which does not affect the aperture photometry since it is equivalent to a constant background in the

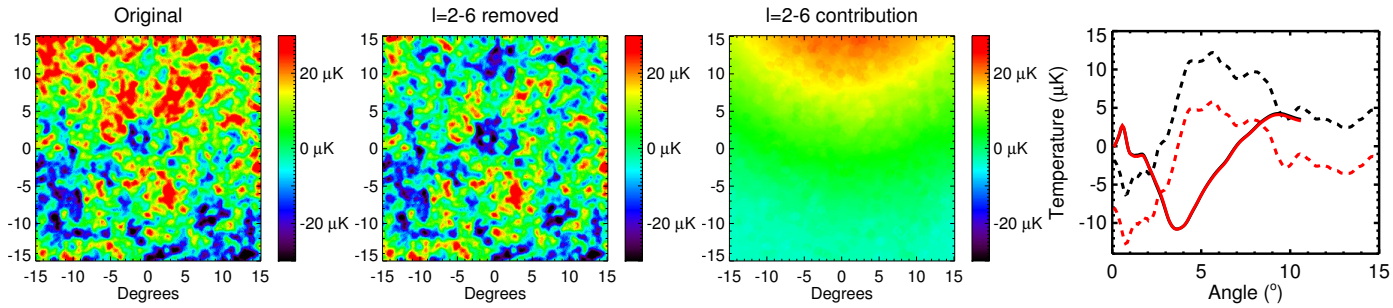

Fig. 5. The three images represent the stacking of the Gr08 voids done (from left to right) on the cleaned WMAP V map, on the same map without its $\ell = 2 - 6$ multipoles, and on these multipoles only. The temperature (dotted curves) and photometry (solid) profiles shown on the rightmost plot are obtained from the first (black curves) and second (red) stacked image. The temperature offset induced by the removed multipoles does not affect the photometry.

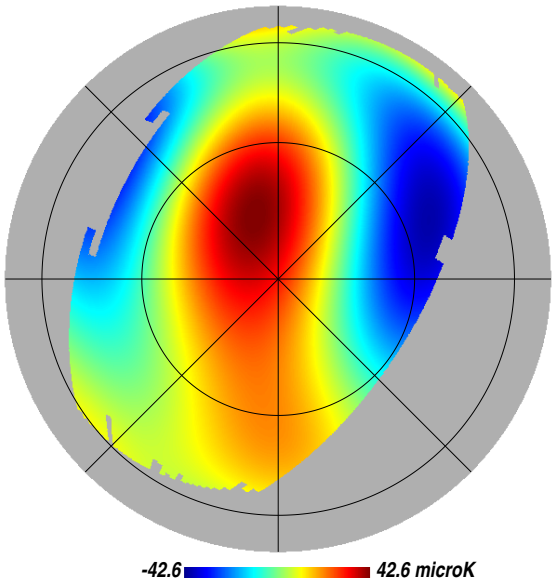

Fig. 6. Orthographic projection of the $\ell = 2$ to 6 multipoles map extracted from the foreground reduced WMAP Q map, in galactic coordinates. Only half of the map is visible (centred on the galactic North pole), with a mask showing only the area covered by the main SDSS. A graticule grid has been superposed with a 45° step in longitude and 30° in latitude.

calculation. For this reason, we will keep using the original CMB maps in our studies, which will also prevent the possible removal of relevant information in other stacked images. We should however keep in mind that the temperature profiles will be affected by a systematic offset as shown in Fig. 5.

3.3. Significance estimation

When taken alone, the stacked images and their associated profiles are not enough to conclude about a possible detection of the iSW effect. Any peculiar feature that seems to stand out could very well be a random event well within statistical fluctuations. As a consequence, we have to take great care in assessing the significance of our results.

We devise a systematic way to compute the significance adopting a Monte Carlo approach. Let us consider the stack of N_v real voids whose significance we try to estimate. We pick many sets (at least 10000) of N_v random positions on the sky confined within the area covered by the SDSS. For each random set, we perform the same analyses as for the real voids, i.e. we produce a stacked image of the N_v patches extracted from the same CMB maps, and compute its radial temperature and photometry profiles. We store all these profiles in memory and end up with thousands of temperature profiles (called here $T^i_{\rm sim}(\theta)$) and photometry profiles ($P^i_{\rm sim}(\theta)$). After this, for every angular size of the profiles, we compare the results from the stack of data voids to the statistical distribution of results from the random stacks. In practical terms, we calculate the signal-to-noise ratio (SNR) of the real temperature ($T_{\rm real}(\theta)$) or photometry ($P_{\rm real}(\theta)$) profiles, at each angle θ considered, as follows :

$$\mathrm{SNR}_{T,P}(\theta) = \frac{\left|(T,P)_{\rm real}(\theta) - \mathrm{Avg}[(T^i,P^i)_{\rm sim}(\theta)]\right|}{\mathrm{StdDev}[(T^i,P^i)_{\rm sim}(\theta)]} \quad (1)$$

where the average and the standard deviation are evaluated over the collection of random stacks. We then obtain two SNR angular profiles for the considered stack: one of its temperature and one of its photometry.

An application of this procedure is illustrated in Fig. 7 and 8 where we assess the significance of our fiducial stack (Gr08 voids) in the CMB of WMAP V band. For this particular example, we used more than 14000 sets of 50 random positions, which seems plenty enough to sample the distribution of temperature and photometry profiles. Indeed this is hinted at by Fig. 8 where the histogram of photometry values at a given angular size follows closely a Gaussian distribution. We will discuss the interpretation of this data in Sections 4 and 5. As far as our procedure is concerned, this estimation of the significance robust is and will be used in the next section for all our results.

4. Results

We apply the procedure described in the previous section to all our stacks in order to estimate their significance. We show the results for the photometry of the stacks for each catalogue and subsample, with an assessment of the significance (Figs. 9, 10 and 11). We also summarise our results in Table 2 where we report for each considered catalogue/subsample the highest measured value of the SNR and its corresponding angular scale, for the three frequency bands used.

4.1. Revisiting Gr08

The work of Gr08 reported a 3.7σ signal in the stacking of their voids at a scale of 4°. With the same dataset we find a reasonable agreement with a preferred scale of $\sim 3.7°$ with an SNR ~ 3.3 (Fig. 8). These differences can be imputed to our use of WMAP 7 maps instead of the WMAP 5 ILC map for Gr08, and to a

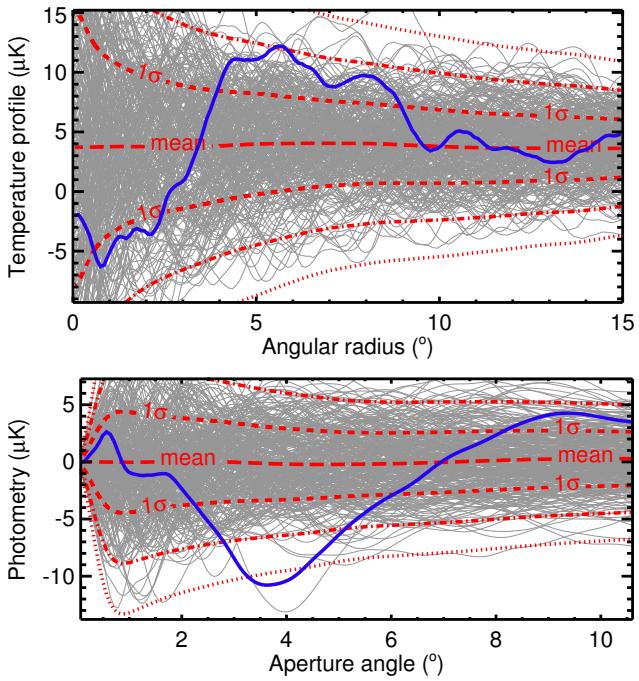

Fig. 7. *Top panel :* For illustration, the thin grey curves are the temperature profiles of just a few hundreds of stacks of 50 random positions. We plotted the mean profile (long red dahes) from all 14000 random stacks and also the 1σ (dashed), 2σ (dash-dotted) and 3σ (dotted) limits of the distribution of profiles. The blue solid curve is the result from the fiducial stacking of Gr08 voids. Every stacking here is carried out in the WMAP V CMB map, smoothed at 30.6'. *Bottom panel :* Same legend as before, for the photometry profiles. Similarly to Gr08, the signal from their voids stands out at more than 3σ around an angular scale of 4°.

Table 2. Summary of our results for all catalogues. The leftmost column contains the name and details of the sample, with the number of voids used. The other columns show the best SNR values of the photometry profiles with their associated angular scales. From left to right, we separate the results from the cleaned Q, V and W maps.

Sample (Number of voids used/ Total number)	**Bests SNR and associated angles**					
	Q band		**V band**		**W band**	
	SNR	Angle	SNR	Angle	SNR	Angle
Granett et al.						
All voids (50/50)	3.23	3.75°	3.33	3.75°	3.32	3.68°
Pan et al.						
Voids with radii lower than 10.6° (1034/1055)	1.01	1.56°	0.87	0.57°	1.14	0.99°
Sutter et al. (voids with radii< 10.6°)						
dim1 (88/97)	1.27	0.57°	1.39	0.85°	1.18	0.92°
dim2 (357/360)	1.27	1.91°	1.00	1.98°	1.18	1.91°
bright1 (287/287)	1.15	1.70°	0.94	1.77°	1.29	1.70°
bright2 (146/146)	2.41	2.40°	2.54	2.40°	2.67	2.40°
lrgdim (221/224)	1.52	2.97°	1.58	2.97°	1.61	2.97°
lrgbright (32/32)	2.19	1.20°	2.03	1.27°	2.11	1.20°

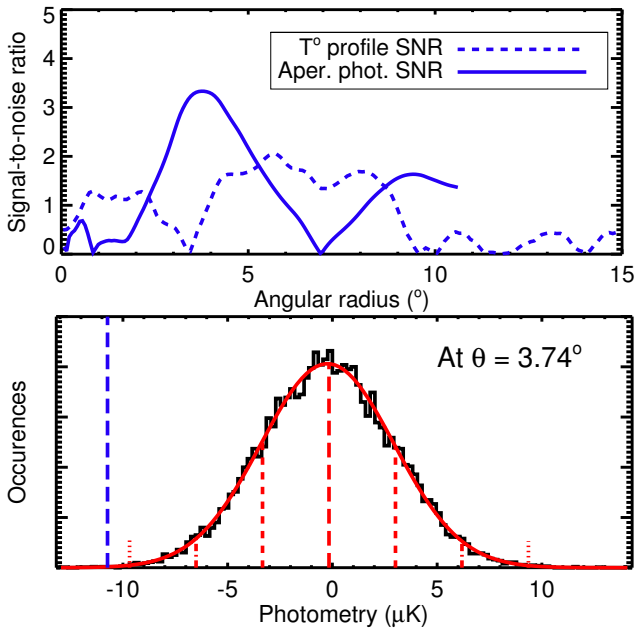

Fig. 8. *Top panel :* Signal-to-noise ratio (as defined in Eq. 1) of the temperature (dashed blue) and photometry (solid blue) profiles of our fiducial stack in WMAP V CMB map. A $\sim 3.3\sigma$ signal stands out in the photometry at a scale of 3.74°. *Bottom panel :* Distribution of photometry values for an aperture angle of 3.74°, from 14000 stacks of 50 random positions. The mean, 1, 2 and 3σ values are marked the same way as in Fig. 7. The blue long-dashed line shows the value obtained from the fiducial stacking. The best fitting Gaussian (red solid curved) follows closely the distribution.

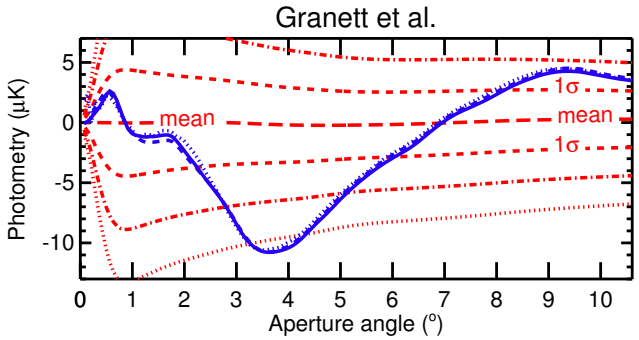

Fig. 9. Photometry profiles from the stacking of Gr08 voids, for the cleaned Q (*dotted blue*), V (*solid blue*) and W (*dashed blue*) CMB map. The significance is illustrated for the V band only with the 1, 2 and 3σ limits (*red curves*) in the same way as Fig. 7.

lesser extent to light differences in the stacking procedure, profile calculations or significance estimation. While we can argue its cosmological origin, the signal seems to be persisting and is essentially identical across frequencies (see Fig. 9) as expected of the iSW effect. However, we discovered an important feature in the temperature profile of the stacked image and its significance. Indeed, in the top panel of Fig. 7 we see that the central cold spot of the signal (below 3.5°) does not particularly stand out compared to random stacks (1σ significance only). On the other hand, we measure around the spot a wide hot ring with higher significance (up to 2σ) at scales between 3.5° and 10°. The impact of this ring is even visible in the photometry profile at higher scales, with its significance reaching almost 2σ around 9°.

Interpreting it in the light of the iSW effect, this would imply the presence of much larger overdensities surrounding the already large supervoids. Considering the filamentary structure of our Universe, this situation is unlikely. This peculiarity leads us to question whether the measured central cold spot – physically interpreted as an iSW signal – is really remarkable : it might as well be due to random fluctuations of the CMB, whose

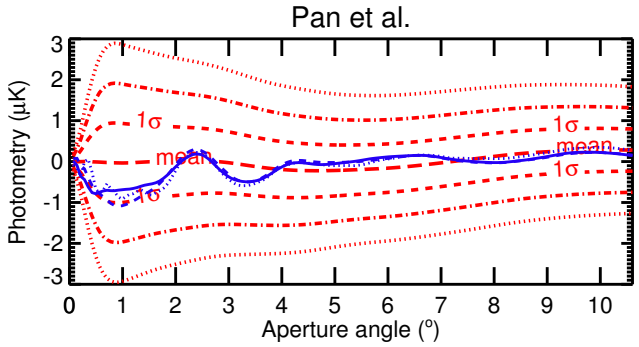

Fig. 10. Photometry profiles from the stacking of Pan et al. voids (same conventions as Fig 9).

significance was coincidentally strengthened by a surrounding hot region in the stacked image.

One could find an argument in favour of the iSW interpretation by noting the good match between the preferred scale in the SNR ($\sim 3.7°$) and the mean effective angular radius of the Gr08 voids ($\sim 3.5°$). As a matter of fact, the same argument can be turned around to rebut this interpretation : We intuit that the iSW effect should fade close to the border of the voids, making the cold spot noticeably smaller than the underlying structure. Moreover, the way it is computed (cf. Section 3.1), the aperture photometry will inherently peak at a scale systematically smaller than the full width of the signal. Before any definitive answer on the matter, this discussion would require a more rigorous investigation, through theory and/or numerical simulations, of the iSW effect expected from such superstructures, which is beyond the scope of this paper.

4.2. Other catalogues

The two other catalogues used in our analysis yield mixed results, with no significance of the same level as the Gr08 catalogue. While discouraging, one has to remember that according to current theoretical predictions, we expect this iSW signal to be difficult to detect, and with low significance only.

The stacking of the 1055 voids of Pan et al. gives a faint signal below the 1σ level (Fig. 10), which does not allow any interpretation. This may be due to the high number of voids in the sample, which has a very wide distribution of angular sizes. We considered the idea of dividing this catalogue (and the Sutter et al. one) into subsamples based on redshift, radius, and/or angular sizes. After several attempts, it did not yield any significant result, and we faced a number of issues regarding possible a posteriori selection effects and the hassle of finding an appropriate size for the subsamples. Indeed, a smaller number of structures implies a narrower range of sizes and redshifts, but it can also greatly reduce the signal-to-noise ratio.

We still addressed this issue partially by analysing separately the six subsamples of Sutter et al. (Fig. 11) – a simple division based on redshift but in principle free from selection effects. The first three subsamples in terms of redshift (*dim1, dim2* and *bright1*) seem to hint very slightly at signal, but only with a 1σ significance at most, and at very small angles. Judging by the high variation of the whole profiles, in which we also detect high-SNR "hot" signals (supposedly associated to overdensities), we cannot conclude about the origin and actual existence of this signal.

The three other profiles reveal more significant results, with signals close to 2σ (for *lrgdim, lrgbright*) and even above for

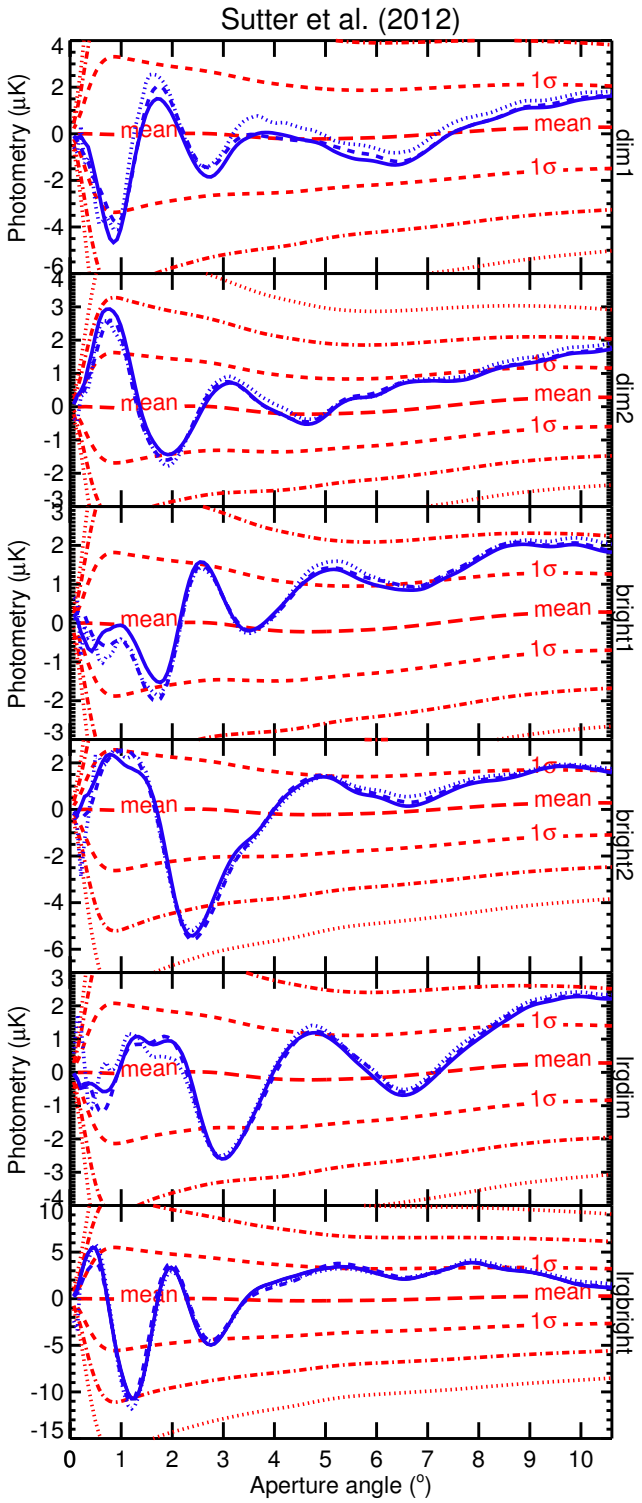

Fig. 11. Photometry profiles from the stacking of Sutter et al. voids and its six subsamples (same conventions as Fig 9).

the *bright2* subsample. Again these signals are found at relatively small angles (between 2 to 3°) but are rather constant in frequency, which is crucial in the search of an iSW signal. Signs of a correlation also appears between these scales and the mean value of the distribution of angular size in these samples, as well as in some of the others (see Table 3). The measured preferred scales are about twice as small as the mean void scale. Considering the iSW effect as the origin of these signals, the difference in scale could be explained by the ellipsoidal nature of

Table 3. Location of the minima in the photometry profile for the stacking of Sutter et al. voids. For each subsample, we indicate the mean angular size of the voids, then report the preferred angular scale(s) and finally their ratio to the mean size. The ratios in bold point out a certain level of correlation between the two sizes.

Void sample	Mean ang. size	Phot. profile minima	Ratio to mean ang. size
dim1	7.06°	0.85°	0.12
		2.76°	**0.39**
dim2	4.34°	1.98°	**0.46**
bright1	4.32°	1.77°	**0.41**
bright2	4.97°	2.40°	**0.48**
lrgdim	6.16°	2.97°	**0.48**
lrgbright	6.55°	1.27°	0.19
		2.76°	**0.42**

the voids and the mixing of many voids sizes in the stacking. Together, they may complicate the prediction of the expected shape and properties of stacked iSW signal from these voids, e.g. making it much smaller than the actual size of the structures. Nevertheless, the the significance of this possible correlation would be hard to estimate.

4.3. Rescaling tests

Since grouping voids by size and/or redshift bins did not prove to be a fruitful way, we tried and adopted another approach in order to enhance the significance of the signal. We kept each subsample in its entirety and did again the stacking analysis, but this time rescaling the voids according to their effective radii. In practical terms, this means cutting the CMB patches so that each void occupies the same space on the stacked image.

We keep the same protocol as described before in Section 3.1, but we change only the resolution of the extracted patches: for each patch, it now depends on the size of the corresponding void. Each time, we cut a square patch with a side six times the size of the void effective radius it contains. Naturally, we also adapt our protocol for the estimation of the significance : the sets of random positions are still drawn the same way, but each random stacking is submitted to the same rescaling as that done on the identified void patches. This will have the effect of mixing different scales in the original CMB map, and will most likely amplify the variance of these random stacks compared to those of Section 3.3.

We begin with the fiducial stacking of the voids of Gr08 : a comparison between the stacked images is illustrated in Fig. 12 while the different profiles are shown in Fig. 13. The signal identified in Section 4.1 still appears after rescaling, with the best significance around scales between 1 and 1.3 times the void effective radii. This value seems somehow a little too high since, as stated above, we expect this value to be around or smaller than 1 (due to the irregular geometry of the voids). The significance of the signal is also found to be lower (SNR$\sim$ 2.8 versus $\sim$ 3.3). This is partly due to the increased variance of the signal (cf. the wider $1/2/3\sigma$ limits in the profiles) induced by the rescaling. But it is also a consequence of the lower amplitude measured for the signal, at odds with our expectations of the rescaling procedure. This could be a further hint that the signal seen in the stacked image may actually be dominated by random CMB fluctuations. On the other hand, the temperature profile of the rescaled stack seems more consistent, with a higher significance cold spot in the centre (cf. first paragraph of Section 4.1 for comparison).

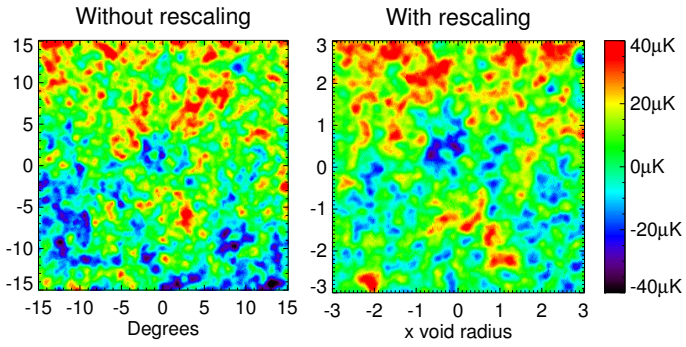

Fig. 12. Stacked images of Gr08 voids, without (*left*) and with (*right*) a rescaling of the CMB patches proportional to the void sizes.

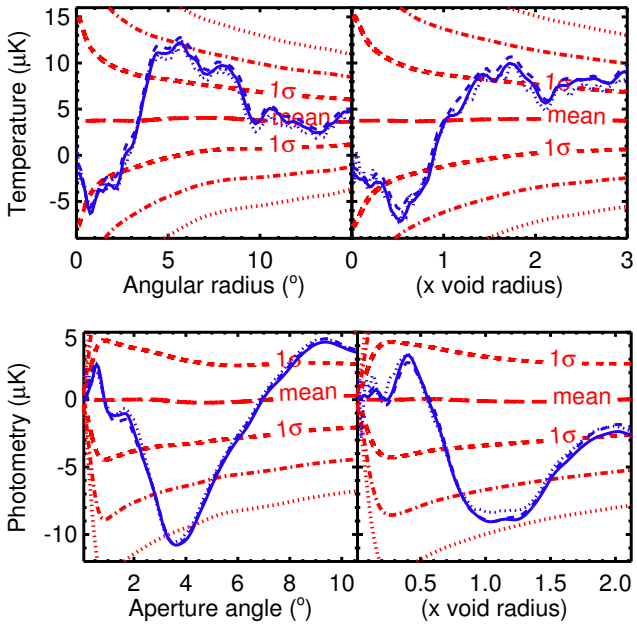

Fig. 13. Temperature (*top*) and photometry (*bottom*) profiles for the original (*left*) and rescaled (*right*) stacking of Gr08 voids (same conventions as Fig 9).

From this first test, we understand that if the rescaling process does not at least improve the absolute amplitude of any previously detected signal, then any subsequent significance estimation is useless since the variance will be necessarily larger and would thus further decrease the SNR. Therefore we first plot a summary of the photometry profiles obtained from the rescaled stacks of Sutter et al. and Pan et al. voids (Fig. 14). Again, no signal of particular importance arises from this new analysis of Pan et al. voids, with amplitudes which do not depart much from the original stacking. Concerning the Sutter et al. catalogue, some signals seem to persist in the rescaled photometry profiles, but only with amplitudes similar to those of the original stacks. Although these are likely to have a weaker SNR, we still evaluate the significance of three of the rescaled profiles (*bright2*, *lrgdim* and *lrgbright*, see Fig. 15) for illustration.

As expected, the new significances have dropped with the rescaling : the rather strong signal in the original *bright2* is now below the 2σ limit but is still located around scales close to half the void sizes (cf. Table 3 and associated discussion). However, its amplitude is no longer entirely consistent across frequencies, casting a doubt on its possible iSW interpretation. A strong signal also seems to be present at the largest scales in the same pro-

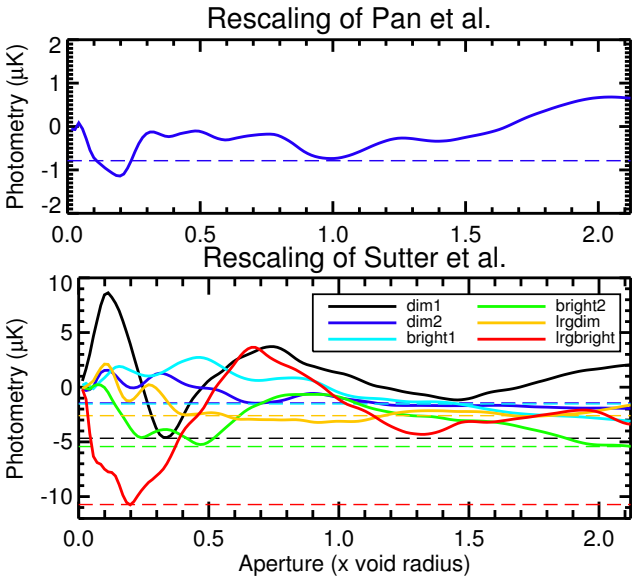

Fig. 14. Summary of the photometry profiles extracted from the rescaled stacks of Pan et al. and Sutter et al. The coloured dashed lines indicate for each sample the lowest amplitude measured in the original stacking ; this is an indication of the usefulness of the rescaling procedure.

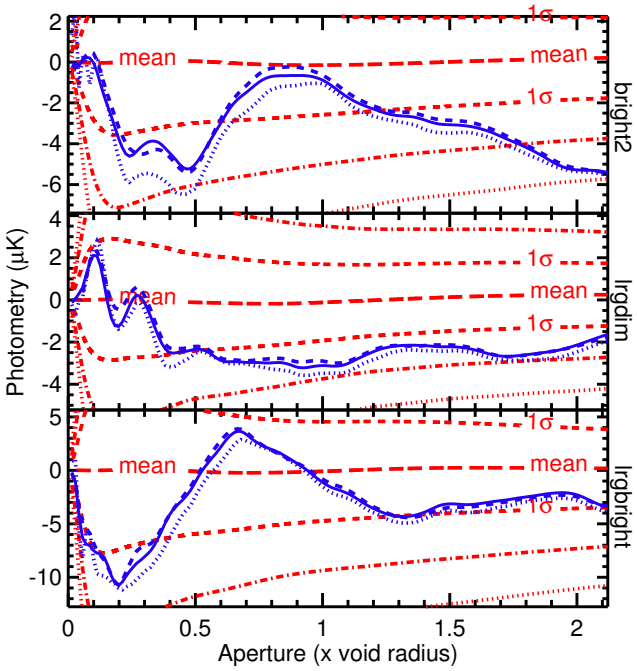

Fig. 15. Photometry profiles and significance for the rescaled stacks of three Sutter et al. subsamples : from top to bottom, *bright2*, *lrgdim* and *lrgbright* (same conventions as Fig 9).

file, but an interpretation or a physical explanation are difficult to find. As for the signal that was found in the original *lrgdim* profile, it appears to be "stretched" over many scales with a significance comparable to what was measured above (between 1 and 2σ). Finally the new *lrgbright* profile only shows one significant result but with the same SNR and again at a very small scale (0.2 times the void sizes), therefore hardly attributable an iSW effect produced by the voids.

In summary, the introduction of a rescaling in the stacking procedure does not yield any improvement on our previous results, which can be interpreted several ways. One possibility is that the hints at signals that we measured above were not entirely the result of the iSW effect produced by voids, but were due mostly to random fluctuations of the CMB temperature that were then "diluted" by the rescaling process, thus the lack of increase in the SNR. Another possibility could be that the stacked iSW signal of so many different voids, spanning broad redshift and size ranges, leaves a signature in the photometry that is non-trivial. However, in order to test this hypothesis, the exact signal expected from such a vast variety of rescaled voids needs to be rigorously computed in the first place.

Lastly, we may argue in favour of the rescaling after seeing that the signal from Gr08 voids seems to be essentially conserved after rescaling (apart from the small decrease in SNR) compared to the other catalogues. However, this has to be put into perspective since the distribution of angular sizes for these voids is much narrower : combined with the small number of voids, the rescaling process (in this particular case) is not expected to have a large influence on the stacked image.

5. Discussion

There are a couple of effects that can make the interpretation of the results difficult and that we should keep in mind. Let us mention at least two of them.

5.1. Selection effects

The results from the previous section highlight the difficulty of getting a clear detection of the iSW effect, at least when using the various catalogues as such. With this in mind, one could be tempted to amplify the signals hinted at by isolating the voids that contribute most. We experimented whit this idea and applied it on the best SNR from our new results in Section 4.2, i.e. the stacking of the *bright2* subsample. From the 146 voids of the original set, we only keep the half (73 voids) that contributes the most to the minima of the photometry profile (at the scale of 2.35°). The resulting photometry profile is plotted in Fig. 16 and indeed shows a dramatic increase in the amplitude of signal. From there, the crux of the matter is to assess the significance of this new result. When using the same procedure as in Section 3.3 (many stacks of 73 random positions), we obtain a surprisingly high SNR, above 8σ. This value clearly overestimates the real significance, as it ignores the selection that we performed on the sample. We need to revise our protocol as follows. We first generate many sets of 146 random positions (instead of 73). Then for each set, we select and stack only the half that contributes most to the photometry profile at the same angular scale of 2.35°. Once we draw enough such random stacks, we keep the rest of the procedure identical. The corrected significance (also plotted in Fig. 16) drops down to a level comparable with the initial SNR (~ 2-2.5) in the original stack (see Fig. 11). Such an a posteriori selection cannot be used to improve the SNR of the final stacked signal.

Actually, taking a closer look at these selection effects, we notice that with only one set of 146 random positions (like those we generated), one can obtain a strong – but completely artificial – signal at almost any desired scale (see Fig. 17) by selecting the appropriate half of it. This further illustrates, and warns us about the risk of a posteriori selections, and does put into perspective any apparently significant signal we obtained. Our results from the new catalogues can be considered safe, as the only form of selection comes from the division of the Sutter et al. voids into redshift subsamples already performed a priori by the authors.

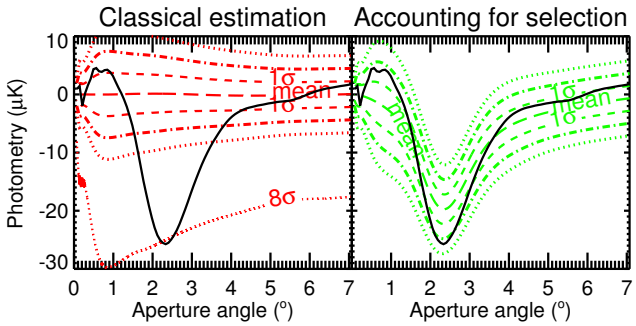

Fig. 16. Photometry profile for the stacking of half the Sutter et al. *bright2* subsample (73 voids from 146), chosen so that the amplitude at 2.35° is the strongest (see text for details). *Left :* the significance is estimated classically. *Right :* the significance accounting for selection effects. The difference between the two significances is obvious and very pronounced.

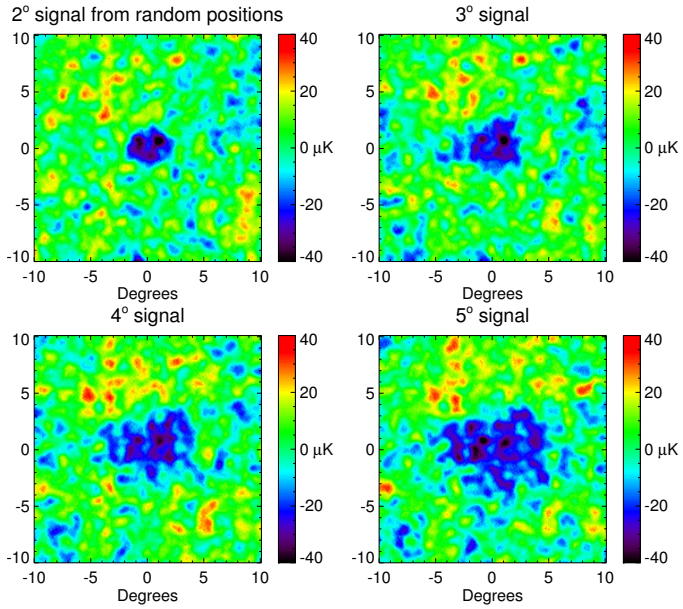

Fig. 17. Illustration of selection effects : from a single set of 146 random positions, we are able to construct a false "iSW-like" signal at any desired scale (here for an angular radius of 2,3,4 and 5°) by selecting and stacking each time the appropriate half of the set.

The Gr08 results are probably also safe, although their 50 voids come originally from a ten times larger sample (see Section 2.2) and were selected according to a density contrast criterium. This selection was also made by the authors prior to looking at CMB data. It is not clear however whether that selection might have helped increasing the SNR artificially.

5.2. Alignment & overlap effects

When interpreting our results, another important issue arises due to the number and location of voids studied. Indeed, these hundreds of voids are confined in the area covered by the SDSS. Since the angular size of these objects often exceeds several degrees, they are bound to fill this area and overlap. As a consequence, each leaves an imprint in the CMB temperature, then the stacking of a set of chosen voids contains in fact contributions from many others. Some structures may also be very close to each other on the sky, further complicating the interpretation of signals.

Table 4. Summary of the overlapping study for the void samples. *First part (top) :* each column indicates for each samples the fraction of its surface that is contaminated by every other sample. *Second part (bottom line) :* Shows for each sample the fraction of its surface where 2 or more voids overlap.

		Fraction of the surface occupied by...							
		Gr08	**Pan**	**Sut-1**	**Sut-2**	**Sut-3**	**Sut-4**	**Sut-5**	**Sut-6**
...in common with ...	**Gr08**	X	14.3%	29.1%	27.4%	27.4%	28.6%	27.5%	29.2%
	Pan	100%	X	100%	100%	100%	100%	100%	100%
	Sut-1	79.4%	39.1%	X	82.0%	82.9%	88.5%	82.8%	96.8%
	Sut-2	87.5%	45.8%	96.2%	X	96.7%	97.3%	92.9%	99.2%
	Sut-3	85.4%	44.7%	94.9%	94.3%	X	96.2%	91.1%	98.9%
	Sut-4	83.6%	41.9%	94.9%	88.9%	90.2%	X	89.2%	98.2%
	Sut-5	89.1%	46.4%	98.4%	94.1%	94.6%	98.9%	X	99.9%
	Sut-6	53.1%	26.1%	64.6%	56.4%	57.7%	61.1%	56.2%	X
		Fraction of overlapping zones							
		13.5%	81.8%	81.3%	88.1%	87.2%	75.5%	86.8%	31.5%

We devise two ways of quantifying these issues :

- First, for each individual sample, we compute both the total area covered by all the voids and the area where at least 2 voids overlap ; we then compute the ratio of these quantities, which represents the "self-contamination" of each sample.
- Then, for every possible pair of samples, we compute the fraction of the area of the first sample shared by the second sample area – a measure of the contamination between samples.

The results are compiled in Table 4. We can see that every sample shows moderate to high contamination with other samples and overlaps itself quite strongly. The results are lower for the Gr08 sample due to the small number of voids. Still, the first row of Table 4 shows that many voids from other catalogues will contribute to the stacking of the Gr08 voids, making it further difficult to interpret its relatively high significance results. This is true for every catalogue of voids identified in the same area : since they overlap, it is difficult to guess which are the objects that give birth to the actual iSW signal.

Both aspects of this study show that contamination from other samples is indeed frequent in the stacking of these voids. Supposedly, we can expect the contamination to cancel out for large numbers of stacked patches. In any case, the probability of measuring a false signal (due to a fortuitous event) may be heightened by the overlapping of so many voids. An accurate simulation of the expected signature from such a collection of overlapping structures will help quantifying these contaminations and their effects on a possible iSW effect detection.

6. Conclusion

In this paper, we revisited the stacking of voids in CMB maps as a potential probe of the existence of Dark Energy through the expected iSW effect from these structures. Previous work by Granett et al. (2008a, Gr08) has measured a 3.7σ signal in WMAP 5 ILC map using a catalogue of 50 selected supervoids extracted from the SDSS (DR6). We devised a complete protocol for a stacking procedure, from a careful choice of maps to a rigorous estimation of the significance. We first applied it to the catalogue of voids of Gr08 and did not find any significant difference, if not a little weaker signal and associated SNR (by 0.4σ). We then extended the analysis to two new void catalogues by Pan et al. (2012) and Sutter et al. (2012) which yielded only hints at signals, not nearly as strong as the Gr08 results, despite

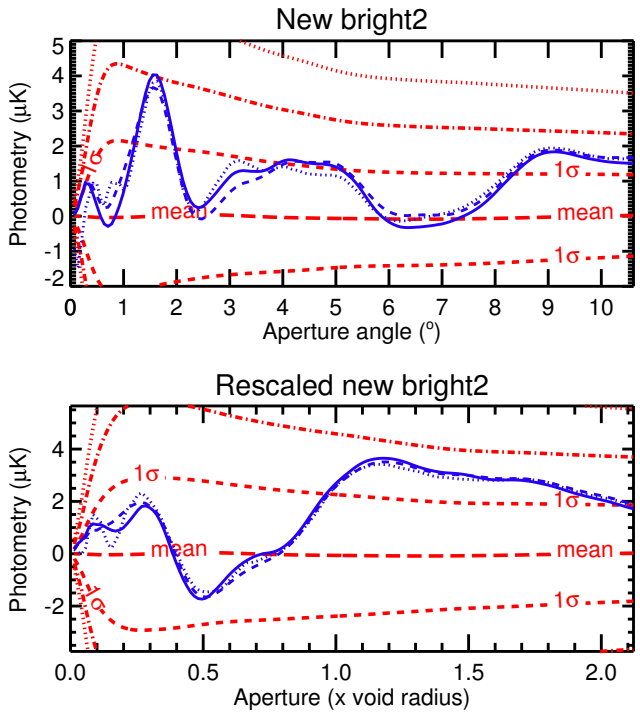

Fig. 18. Photometry profiles and significance of the stacking of the latest Sutter et al. *bright2*, before (top) and after (bottom) rescaling the CMB patches.

the significantly larger number of voids. We noticed nonetheless a trend for the preferred scale in the signal, which seemed to point to half the mean size of the voids used in the stacking. This was not found with the Gr08 voids, for which the highest-significance scale was closer to the mean void size (note however that due to the irregular geometry of the stacked voids, we expect the favoured characteristic scale to be in fact smaller). A rescaling of the CMB patches prior to stacking according to the void sizes did not add anything to the significance and appeared in fact detrimental to most of our results. This includes the Gr08 voids which, in addition, preferred after rescaling yet a larger scale than expected. Along these mixed results, we also addressed the risks of possible selection effects that could lead easily to an overestimation of the significance. We also stressed that the surface density of the voids within the SDSS area make them overlap significantly, making it even more difficult to formulate clear expectations about, and interpretations of the measured signals. Finally, it is known that voids are actually difficult to identify with certainty. For instance, while being identified in the same SDSS DR7 set, the void subsambles *dim1* and *dim2* of Sutter et al. lie within the same redshift range as the voids identified by Pan et al., but they cover quite a different range in size and are differently distributed in redshift. We argue that, combined with the unavoidable overlap of voids along a line of sight mentioned above, this makes premature any claim that the iSW-like signal detected by the stacking of voids is at odds with ΛCDM.

As a final remark, let us note that during the redaction of this paper, an update of the Sutter et al. catalogue appeared on-line.[4] The changes were described as minor and stated as having no impact on the conclusions of the associated paper (Sutter et al. 2012). We examined rapidly the new catalogue, and noticed that in fact the number of voids reported was 50% bigger. This is due to the fact that numerous small voids were newly detected, thanks to an improved void finding algorithm. Upon closer examination, a few voids from the old catalogue are now missing, and many others have seen modifications in their redshifts, sizes and positions on sky, ranging from minor changes to more drastic ones. The entire *lrgbright* subsample has changed almost completely with a much larger scatter in sizes and redshifts. This update of course does have a significant impact on the stacking of the voids, especially through the inclusion of the new small voids. We illustrate it in Fig. 18 which contains the photometry profile of the stacking done on the new *bright2* subsample, on which we had obtained our most significant signal.

As can be seen here the original signal is completely lost. The photometry profile shows only positive amplitudes, incompatible with an iSW signal from voids. This is probably due to the new small voids (58 added to the original 146) and – to a lesser extent – to the shifts in the positions of the original voids. Rescaling the voids does somewhat improve the results (see also Fig. 18), but yields only a faint signal, again around half the typical size of the voids involved. An examination of the other subsamples gives similar results, both on the loss of any previously detected signal in the photometry profile and on the minor improvement obtained through the rescaling process.

Acknowledgements. We acknowledge discussions with C. Hernández-Monteagudo and J. M. Diego at an early stage of this work. We also thank N. Aghanim and F. Lacasa for stimulating discussions. Some of the results in this paper have been derived using the HEALPix (Górski et al. 2005) package. The work of S. Ilić is funded by the Doctoral Programme 'AAP 2010 contrats doctoraux Paris-Sud 11'.

References

Adelman-McCarthy, J. K., Agüeros, M. A., Allam, S. S., et al. 2008, ApJS, 175, 297
Aghanim, N., Majumdar, S., & Silk, J. 2008, Reports on Progress in Physics, 71, 066902
Boughn, S. P. & Crittenden, R. G. 2002, Phys. Rev. Lett., 88, 021302
Boughn, S. P., Crittenden, R. G., & Turok, N. G. 1998, New A, 3, 275
Crittenden, R. G. & Turok, N. 1996, Phys. Rev. Lett., 76, 575
Dupé, F.-X., Rassat, A., Starck, J.-L., & Fadili, M. J. 2011, A&A, 534, A51
Flender, S., Hotchkiss, S., & Nadathur, S. 2012, arXiv:1212.0776
Giannantonio, T., Crittenden, R., Nichol, R., & Ross, A. J. 2012, MNRAS, 426, 2581
Giannantonio, T., Scranton, R., Crittenden, R. G., et al. 2008, Phys. Rev. D, 77, 123520
Górski, K. M., Hivon, E., Banday, A. J., et al. 2005, ApJ, 622, 759
Granett, B. R., Neyrinck, M. C., & Szapudi, I. 2008a, ApJ, 683, L99
Granett, B. R., Neyrinck, M. C., & Szapudi, I. 2008b, arXiv:0805.2974
Granett, B. R., Neyrinck, M. C., & Szapudi, I. 2009, ApJ, 701, 414
Hernández-Monteagudo, C. & Smith, R. E. 2012, arXiv:1212.1174
Hinshaw, G., Weiland, J. L., Hill, R. S., et al. 2009, ApJS, 180, 225
Ho, S., Hirata, C., Padmanabhan, N., Seljak, U., & Bahcall, N. 2008, Phys. Rev. D, 78, 043519
Hoyle, F. & Vogeley, M. S. 2002, ApJ, 566, 641
Hunt, P. & Sarkar, S. 2010, MNRAS, 401, 547
Jarosik, N., Bennett, C. L., Dunkley, J., et al. 2011, ApJS, 192, 14
Kofman, L. A. & Starobinskii, A. A. 1985, Soviet Astronomy Letters, 11, 271
Nadathur, S., Hotchkiss, S., & Sarkar, S. 2012, JCAP, 2012, 042
Neyrinck, M. C. 2008, MNRAS, 386, 2101
Neyrinck, M. C., Gnedin, N. Y., & Hamilton, A. J. S. 2005, MNRAS, 356, 1222
Pan, D. C., Vogeley, M. S., Hoyle, F., Choi, Y.-Y., & Park, C. 2012, MNRAS, 421, 926
Pápai, P. & Szapudi, I. 2010, ApJ, 725, 2078
Pápai, P., Szapudi, I., & Granett, B. R. 2011, ApJ, 732, 27
Sachs, R. K. & Wolfe, A. M. 1967, ApJ, 147, 73
Springel, V., White, S. D. M., Jenkins, A., et al. 2005, Nature, 435, 629
Sutter, P. M., Lavaux, G., Wandelt, B. D., & Weinberg, D. H. 2012, ApJ, 761, 44

Institut d'Astrophysique Spatiale, UMR8617, Université Paris Sud & CNRS, Bât. 121, Orsay F-91405, France

[4] http://www.cosmicvoids.net, 17/11/2012 version.